Society For Biomaterials

In vitro and *in vivo* biological characterization of poly(lactic acid) fiber scaffolds synthesized by air jet spinning

Marco Vladimir Granados-Hernández,[1,2] Janeth Serrano-Bello,[1] Juan José Montesinos,[3] Carlos Alvarez-Gayosso,[4] Luis Alberto Medina-Velázquez,[5,6] Octavio Alvarez-Fregoso,[7] Marco Antonio Alvarez-Perez[1]

[1]Laboratorio de Bioingeniería de Tejidos; DEPel, Facultad de Odontología, UNAM. Circuito Exterior s/n. Cd. Universitaria, 04510 Coyoacán, CDMX, México
[2]Posgrado en Ciencias Biológicas, Universidad Nacional Autónoma de México; Av. Ciudad Universitaria 3000, C.P. 04360, Coyoacán, CDMX, México
[3]Mesenchymal Stem Cells Laboratory, Oncology Research Unit, Oncology Hospital, National Medical Center, IMSS, Mexico City, México
[4]Laboratorio de Materiales Dentales; DEPel, Facultad de Odontología, UNAM. Circuito Exterior s/n. Cd. Universitaria, 04510 Coyoacán, CDMX, México
[5]Instituto de Física, Universidad Nacional Autónoma de México, CDMX 04510, México
[6]Unidad de Investigación Biomédica en Cáncer INCan/UNAM, Instituto Nacional de Cancerología, CDMX 14080, México
[7]Instituto de Investigaciones en Materiales, Circuito Exterior s/n. Cd. Universitaria, 04510 Coyoacán, CDMX, México

Received 6 April 2017; revised 3 November 2017; accepted 12 November 2017
Published online 30 November 2017 in Wiley Online Library (wileyonlinelibrary.com). DOI: 10.1002/jbm.b.34053

Abstract: Poly(lactic acid) (PLA) is one of the most promising renewable and biodegradable polymers for mimic extracellular matrix for tissue engineering applications. In this work, PLA spun membrane scaffold were successfully prepared by air jet spinning technology. Morphology, mechanical properties, *in vitro* biocompatibility, and *in vitro* and *in vivo* degradation of PLA fibrous scaffold were characterized by X-ray diffraction, Fourier Transform Infrared, and scanning electron microscope (SEM). Morphological results assessed by SEM analyses indicated that PLA scaffolds possessed an average fiber diameter of approximately 0.558 ± 0.141 μm for 7% w/v of PLA and approximately 0.647 ± 0.137 μm for 10% w/v. Interestingly, our results showed that the nanofiber size of PLA scaffold allow structural stability after 100 days of *in vitro* degradation in Ringer solution where the average fiber diameter were of approximately 0.633 ± 0.147 μm for 7% w/v and approximately 0.645 ± 0.140 μm for 10% w/v of PLA. Mechanical properties of PLA fibers scaffold after *in vitro* degradation showed decrease in terms of flexibility elongation, and less energy was needed to achieve maximal elastic deformation. The fiber size exerts an influence on the biological response of human Bone Marrow Mesenchymal Stromal Cells as confirmed by MTT assay after 9 days of cell culture and the *in vivo* degradation assay of 7% w/v and 10% w/v of PLA scaffold, did not demonstrate evidence of toxicity with a mild inflammatory respond. In conclusion, airbrushing technology promises to be a viable and attractive alternative technique for producing a biocompatible PLA nanofiber scaffold that could be considered for tissue engineering regeneration. J Biomed Mater Res Part B: Appl Biomater 106B: 2435–2446, 2018.

Key Words: PLA, air jet spinning, *in vitro* and *in vivo* degradation assay, nanofibers, SEM, FTIR, XRD, biocompatibility, MTT assay, tissue engineering

How to cite this article: Granados-Hernández, MV, Serrano-Bello, J, Montesinos, JJ, Alvarez-Gayosso, C, Medina-Velázquez, LA, Alvarez-Fregoso, O, Alvarez-Perez, MA. 2018. *In vitro* and *in vivo* biological characterization of poly(lactic acid) fiber scaffolds synthesized by air jet spinning. J Biomed Mater Res Part B 2018:106B:2435–2446.

INTRODUCTION

In tissue engineering, a biodegradable scaffold plays an important role in mimicking the extracellular matrix (ECM) delivering cells to the wound site, allowing cellular growth and preserving the space for the new tissue formation.[1] The ideal scaffold for tissue engineering should have a three-dimensional structure, be easy to handle, possessing a minimal inflammatory response, with appropriated mechanical and physicochemical properties, and with biodegradable time process, that permits tissue regeneration.[2]

One of the main concern in tissue regeneration is to design a scaffold that could mimic the fibrillar structure of native ECM architecture.[3,4] In recent years, in order to produce scaffolds with nanofibrous morphology, electrospinning

Correspondence to: J. Serrano-Bello; e-mail: janserbe@comunidad.unam.mx or M. Antonio Alvarez-Perez; e-mail: marcoalv@unam.mx
Contract grant sponsor: Dirección General de Asuntos del Personal Académico, Universidad Nacional Autónoma de México, DGAPA-UNAM-PAPIIT; contract grant numbers: IT203618 and IN210815

is a widely used technology that utilizes electrical forces to produce polymer fibers with diameters ranging from 2 nm to several micrometers, employing polymer solutions of both natural and synthetic polymers depending on fabrication parameters such as polymer solvent, polymer concentration, voltage, and collector distance.[5–7] Fabricated fibrous scaffolds by means of electrospinning give rise to several properties such as interconnected porosity, pore size, and fiber size, which stimulate the cell response, such as change in cell morphology, cell attachment, cell proliferation, and cell differentiation.[8–10]

An alternative novel technology for fabricating polymeric fibers scaffolds have been reported in literature and is referred as air-jet spinning (AJS) or solution blow spinning.[11–13] This method utilizes a specialized spinning system nozzle, such as a commercial airbrush, a surface for collecting polymer fibers, and compressed gas through which the polymer solution and a pressurized gas are simultaneously ejected to form the fiber morphology.[14–16] This technique produces fibers within the same size range as electrospinning, and fiber morphology may be controlled by several parameters, such as polymer concentration, surface tension, working distance, spinning gas, temperature, gas pressure, and evaporation rate.[17–19] Air-spinning technology has several advantages as is faster and easy to use, less expensive, safety because it does not employ high voltage, scalability, and versatility in the choice of solvent, and it is applied to produce micro/nanoscale fibers from different synthetic and natural polymers.[12–21] Among all the polymers used by air-spinning technique, poly(lactic acid) (PLA) has been the object of considerable attention due to its great potential in biomedical applications, because it is a biodegradable, biocompatible, and compostable material, making it a good candidate for tissue engineering regeneration.[22,23] Moreover, an interesting study of *in vitro* degradation rate and long-term cytotoxicity behavior of poly(L-lactide) acid (PLLA) by Sabbatier et al.[24] utilizing the air-spinning technique to prepare a PLLA scaffold has previously been reported for vascular tissue engineering applications. Furthermore, the degradation products of PLA are metabolizable and known to be nontoxic to living organisms, and of still greater importance is that it is a U.S. Federal Drug Administration approved polymer, which can be dissolved and easily processed for reconstruction of bone, soft tissue and drug-delivery systems.[22,23,25]

The goal of our present study was to provide the potential of the air-spinning technique for fabricating a fiber membrane scaffold of a polymer solution of PLA focusing on surface characterization, mechanical properties, and the *in vitro and in vivo* degradation behavior of the fabricated air-spun membrane scaffold.

MATERIALS AND METHODS

Poly(lactic acid) pellets ($C_3H_6O_3$; molecular weight (MW) 192,000, called Ingeo 2003D) were purchased from Promaplast, Mexico. Chloroform ($CHCl_3$) and ethyl alcohol absolute anhydrous (CH_3CH_2OH) were supplied by J. T. Baker. All products were utilized as received without further purifications. Polymeric solutions of 7% w/v and 10% w/v of PLA, respectively, were prepared as follow: dissolved PLA in chloroform and stirring by 20 h and after that, ethanol was added, and the solution was stirred for 30 min to obtain a homogeneous solution. The volume ratio of chloroform/ethanol was 3:1.

Preparation of spun membranes

Fibrous spun scaffolds were produced through the AJS process of PLA polymeric solutions of 7% w/v, and 10% w/v. In all cases, the polymeric solution was placed into a commercially available airbrush ADIR model 699 with a 0.3-mm nozzle diameter with a gravitational feed of the PLA solution to synthesize the fiber membrane scaffold. The airbrush was connected to a pressurized argon tank (CAS number 7740-37, concentration >99%, PRAXAIR Mexico) and, for fiber deposition, a pressure of 30 psi with 11 cm of distance from the nozzle to the target was maintained constant. Optimized parameters of the volume of the polymer solution rate with respect to a deposit time of 0.27 mL/min was determined for high-quality fibers deposit.

Airbrushed fiber scaffold characterization

Fibers structures were determined by X-ray diffraction (XRD) employing a D8 Focus Bruker AXS diffractometer with Cu-kα radiation in the 2Θ range between 10 and 35°. The chemical structure of the fibers was analyzed by Fourier Transform Infrared (FTIR) spectroscopy employing an IRAffinity-1S (Shimadzu) within the 400–4000 cm^{-1} range. The morphology and structure of the fibers were observed with a field emission scanning electron microscope (FE-SEM, JSM-7800F, JEOL). Fiber diameter was measured from SEM micrographs employing image analysis software (Image J. National Institutes of Health, Rockville, MD).

In vitro degradation

Five PLA spun membrane scaffolds of 7% w/v and 10% w/v concentration were placed individually into glass vials containing 25 mL Ringer solution ($CaCl_2$ and $C_3H_5O_3{\cdot}Na$, pH 6.36) for the experimental group and bi-distilled water (pH 8.16) for the control group. All samples were maintained in ovens at 37°C until 100 maximum days of the incubation time. After incubation time, the samples were extracted with tweezers, thoroughly washed with deionized water and placed into empty vials to be incubated in a vacuum for 60 min for drying. Afterward, the mechanical properties were analyzed for the scaffolds and for the surface characterization of the scaffolds were analyzed by SEM and FTIR.

Mechanical properties

Rectangular membrane scaffolds of PLA (7% w/v and 10% w/v) of 5 × 20 mm were placed individually into glass vials containing 65 mL Ringer solution for the experimental group and bi-distilled water for the control group. All the samples were maintained in ovens at 37°C until a maximum of 100 days. After this time, the samples were extracted with tweezers, thoroughly washed with deionized water and placed into empty vials to be incubated in a vacuum for 60

min for drying. Subsequently, elastic modulus and resilience were evaluated using the universal mechanical test machine (INSTRON mod. 5567) under ambient conditions, at a test speed of 10 mm/min.

Stress-strain curves were calculated using the forces values obtained by a load cell of 5 kN and displacement values along with the geometric parameters of the samples. Stress (σ) was calculated in MPa according to the following formula: $\sigma = F/A$, where F is the applied load in Newton and A is the area of the sample in mm^2. Strain ([mm/mm]) of the sample was calculated as: $= \Delta L/L_0$, where ΔL is the displacement in mm and L_0 is the initial length of the sample (10 mm).

Elastic modulus was calculated from the slope of the linear section of the stress-strain curve (elastic zone). Resilience ($\mu J/mm^3$) was calculated as area-under-the-linear-section of the stress-strain curve for PLA spun membrane scaffolds. Five membranes of PLA were used for each mechanical experiment and a control group was used as replicates tested for mechanical properties.

Isolation and culture of MSCs derived from bone marrow

The bone marrow (BM) sample was obtained from a volunteer donor according to the ethical guidelines of the Villacoapa Hospital, Mexican Institute for Social Security in Mexico City. Isolation of mononuclear cells (MNCs) from BM was performed as previously described.[26] MNCs from BM were resuspended in low glucose Dulbecco's Modified Eagle's Medium (Gibco, Rockville, MD) that was supplemented with 10% Fetal Bovine Serum (FBS, Gibco BRL) 4 m*M* L-glutamine, 100 U/mL of penicillin, 100 μg/mL of streptomycin, and 100 μg/mL of gentamicin (all reagents were obtained from GIBCO); the cells were seeded at a density of 0.2×10^6 cells/cm^2 in T-25 culture flasks (Corning/Costar, New York). After a 4-day culture, the nonadherent cells were removed and fresh medium was added to the cultures. Once the cultures reached 80% confluence, the cells were harvested with trypsin (0.05% trypsin, 0.53 m*M* EDTA; Gibco) and subcultured at a density of 2000 cells/cm^2 in T-75 flasks (Corning). During the second passage, the cells were harvested, analyzed, and cryopreserved for future use.

Morphological analysis

To identify the morphology of mesenchymal stromal cell (MSC) obtained from BM, second-passage cells were grown in a Petri dish (Corning) at a density of 4000 cells/cm^2. After 6 days of cell culture, cells were stained with toluidine blue (Sigma-Aldrich, St Louis, MO) and examined under a phase-contrast microscope.

Characterization of MSCs

MSC immunophenotypic characterization and differentiation capacities were performed according to previously described protocols.[27] Fluorescein isothiocyanate (FITC), phycoerythrin (PE), or allophycocyanin (APC)-conjugated monoclonal antibodies against CD73, CD90, and CD45 (BD Biosciences, San Diego, CA) CD105, CD13, CD14 (Caltag, Buckingham, UK) HLA-ABC human leukocyte antigens A, B, C, (HLA-ABC) and human leukocyte antigens D, R (HLA-DR) major histocompatibility (MHC) antigens, CD31, and CD34 (Invitrogen, Carlsbad, CA) were employed for flow cytometric analysis of cultured MSC. A total of $1–2 \times 10^5$ cells, previously blocked with Fc receptor blocker (Blocking Reagent Human; Miltenyi Biotec) were resuspended in 100 mL of phosphate-buffered saline (PBS) with 3% FBS and 1 m*M* EDTA and incubated with the appropriate antibodies for 20–30 min; the cells were subsequently washed with 1 mL of PBS (with 3% FBS and 1 m*M* ethylenediaminetetraacetic acid (EDTA)) and fixed with fluorescence-activated cell sorting (FACS) Lysing Solution (BD Biosciences). The labeled cells were analyzed in a Coulter Epics Altra Flow Cytometer (Beckman Coulter, Brea, CA) and at least 10,000 events were collected per sample. The data were analyzed with FlowJo 2.6 software (FlowJo LLC, Ashland, OR).

Adipogenic and osteogenic differentiation was induced with Stem Cells Kits™ (STEMCELL Technologies, Vancouver, BC, Canada). Adipogenic differentiation was determined by visualizing the presence of Oil Red O-stained (Sigma-Aldrich, St. Louis, MO) lipid vacuoles. Osteogenic differentiation was assessed by alkaline phosphatase staining. Chondrogenic differentiation was induced with a commercial induction medium (Cambrex Bio Science, Walkersville, MD) that was supplemented with 10 ng/mL of transforming growth factor beta (TGF-β) (Cambrex). The resulting micromasses were fixed, embedded, and sliced. cross-sections were stained with Alcian blue dye (Sigma-Aldrich) for visualization the chondrogenic differentiation.

Cell culture

Biological assays were performed using human Bone Marrow Mesenchymal Stromal Cells (hBM-MSC) cultured in 75 cm^2 cell-culture flask in Eagles alpha minimum essential medium (α-MEM) supplemented with 10% FBS in antibiotic solution (streptomycin 100 μg/mL and penicillin 100 U/mL, Sigma Chem) and 2 m*M* L-glutamine.

Cytotoxicity test

In vitro indirect cytotoxicity assays were performed using hBM-MSC. Cells were previously seeded at 1×10^4 cells/mL onto 24-well cell-culture plates in triplicate and incubated in α-MEM supplemented with 10% FBS, antibiotic solution (streptomycin 100 μg/mL and penicillin 100 U/mL, SIGMA) and 2 m*M* L-glutamine. Prior to the *in vitro* cytotoxicity test, PLA fiber mats of 7% w/v and 10% w/v (cut into a disk shape of 8 mm of diameter) were incubated individually with 1 mL of α-MEM solution and placed on a rotating mixer at 37°C for a period of 3, 5, 7, and 9 days in triplicates. After this time, 500 μL of the eluent was pipetted onto the seeded hBM-MSC cells, while the cytotoxic control culture was obtained by spiking the cells with the same amount of α-MEM containing 10% ethanol. The cell culture plates were further incubated at 37°C for 48 h for each experimental time. Cell metabolic activity was evaluated by employing the MTT assay. This assay is based on the ability

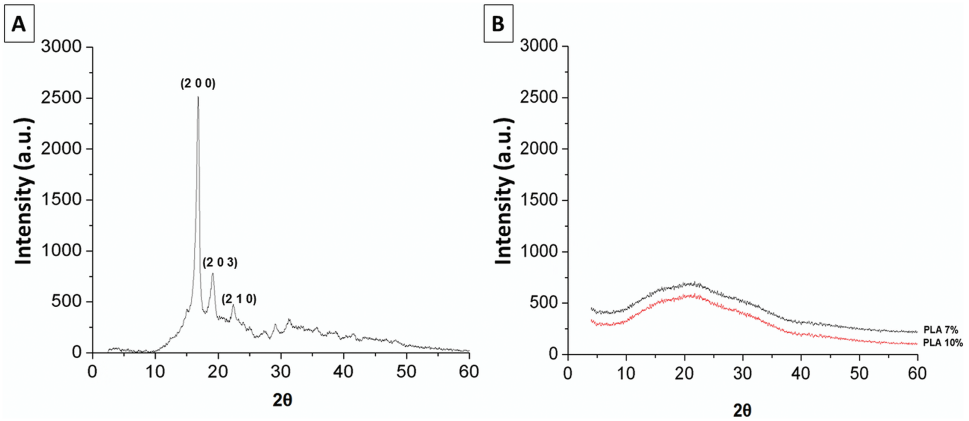

FIGURE 1. XRD patterns of (A) PLA pellet and (B) nanofibers spun mats of PLA (7% w/v and 10% w/v).

of mitochondrial dehydrogenases of living cells to oxidize a tetrazolium salt (3-[4,5-dimethylthiazolyl-2-y]-2,5-diphenyl-tetrazolium bromide, MTT) into an insoluble blue formazan product. The concentration of the blue formazan product is directly proportional to the number of metabolically active cells. hBM-MSC incubated with supernatant of experimental scaffolds were incubated with 0.5 mg/mL of MTT for 4 h at 37°C. The supernatant was removed and 200 μL of dimethyl sulfoxide (DMSO) was added to each well. After 60 min of slow shaking, absorbance was quantified by spectrophotometry at 570 nm with a plate reader. All indirect cytotoxicity assay experiments were made in triplicate.

Cell viability

hBM-MSC were plated at concentration of 1×10^4 cell/mL in triplicate onto a disc shape of 8 mm of diameter of 7% w/v and 10% w/v of PLA spun fiber mats. Cell viability were checked after 3, 5, 7, and 9 days of culture by MTT assay. hBM-MSC cell cultures after these time periods were incubated with 0.5 mg/mL of MTT for 4 h at 37°C. Then, the supernatant was removed and 200 μL of DMSO was added to each well. After 60 min of slow shaking, absorbance was quantified by spectrophotometry at 570 nm with a plate reader. Conventional polystyrene 24-well culture plates were utilized as control. During the experiment, the culture medium was changed every 2 days for fresh media, and all viability experiments were conducted in triplicate.

In vivo degradation

Ethics statement. All animal procedures were approved by the Institutional Research, Ethical, and Animal Care and Use Committee of the Faculty of Dentistry of the National Autonomous University of Mexico (UNAM).

Implantation of scaffolds in animals. Twenty-four adult male Wistar rats, 12 weeks of age and weighting of 250 g each, were obtained from the vivarium of the Medical Faculty, UNAM. These animals were randomly divided into six groups of four rats each, corresponding to the established time periods (8, 20, 40, 60, 80, and 100 days). All animal groups were surgically implanted with scaffolds under general anesthesia (Ketamine 80 mm/kg and Xylazine 10 mg/kg). Before implantation of the scaffold, the surgical site was prepared by shaving and cleaning with disinfectant. Three triangular flaps of approximately 2 cm were made: one on the upper right where the 7% w/v of PLA scaffold was placed; one on the left where the 10% w/v PLA scaffold was placed, and on the lower Gelfoam® was placed as control scaffold. Each scaffold was sutured to the dermis with 5–0 Nylon to stabilize them in order to not lose them or to avoid movement from its position. All animals were housed in purpose-designed rooms at a temperature 18–22°C with a 50% of relative humidity under conditions of 12 h of photoperiod (light/dark) cycles. The animals had ad libitum access to water and standard laboratory diet. A postsurgical clinical follow-up was carried out, assessing the general condition of the animal, wound appearance, bleeding, exudate, or extrusion of the scaffolds.

Ex vivo preparation of scaffolds for histological characterization. The animals were sacrificed at various time points (8, 20, 40, 60, 80, and 100 days) using a CO_2 chamber; the scaffolds were dissected from the rat to include surrounding soft tissue, the samples were placed in formalin prior to histological processing and were then stained with hematoxylin and eosin (H&E) to evaluate inflammatory response and with Masson trichrome to evaluate fibrosis and degradation.

Statistical analysis

The *in vitro* tests were statistically evaluated, and statistical values are expressed as mean ± standard error. Multiple comparisons between groups were conducted with the Bonferroni *post hoc* test with a one-way analysis of variance and with a $p < 0.05$ considered statistically significant. Statistical analyses were performed with SPSS ver. 20.0 statistical software (IBM).

RESULTS

X-ray diffraction

X-ray diffraction results showed the crystalline phase of the bulk PLA before being deposited by AJS process and used

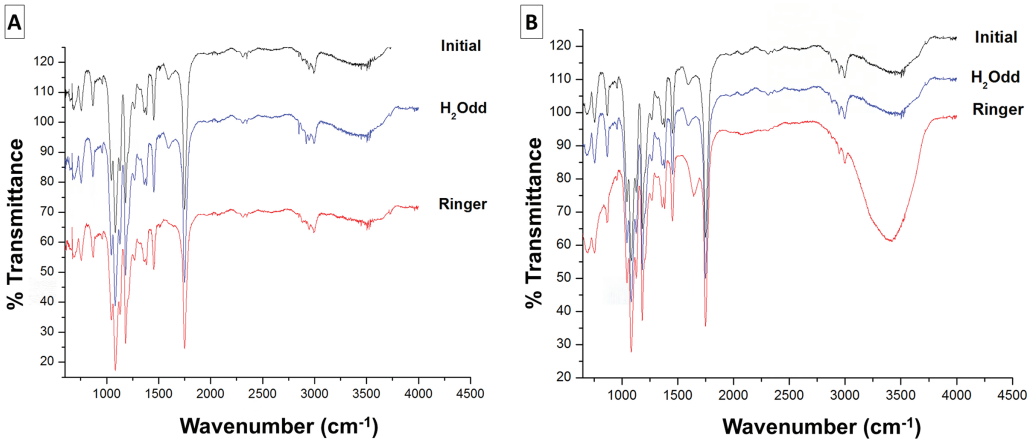

FIGURE 2. FTIR spectra of PLA 7% w/v (A) and 10% w/v (B) before and after 100 days of *in vitro* hydrolytic degradation on bidistilled water and Ringer solution.

as reference [Figure 1(A)]. XRD of bulk PLA exhibited a crystalline structure with peaks at 16.7, 19.1, and 22.4° 2Θ distances, these peaks are characteristic of the α-form orthorhombic structure according to PDF-2–2006 card number 00–054-1917, Diffract Plus 2005.[28,29] After stretching the PLA solution of 7% w/v and 10% w/v concentration by air-jet technique during the synthesis of randomly oriented fiber membranes, the XRD of PLA fibers presented an amorphous structure [Figure 1(B)].

Fourier transform infrared

The chemical structures of PLA fiber membranes synthesized with different concentration of [7% w/v, Figure 2(A)] and [10% w/v, Figure 2(B)] were obtained using FTIR spectroscopy, previously washed with deionized water to avoid interaction between the buffer and the sample and compared to identify structural changes by means of the effect of the *in vitro* degradation test.[30]

Infrared spectra absorption demonstrated the characteristic bands of PLA spectrum assignments as mentioned in literature: Ester-carbonyl group main vibrational-band absorbance peak was localized at 1750 cm^{-1}; C-H bending vibrations of CH_3 were at 1445 and 1380 cm^{-1}; C-H bending vibrations of carbonyl CH were at 1350 cm^{-1}; backbone stretching and CH_3 rocking-band region was at 960–830 cm^{-1}; CH symmetric and asymmetric stretch region was observed at 3200–2800 cm^{-1} and the bands assigned to the C-O stretch of lactide were at 1260 and 1100 cm^{-1}, respectively.[31–33] Comparison of infrared (IR) spectra after *in vitro* degradation test in bi-distilled water and Ringer solution of PLA fiber membranes of 7% w/v and 10% w/v exhibited some quite similar spectra from 600 to 4500 cm^{-1}. However, there were some regions of the spectra that revealed a slight increase and decrease of approximately 11% in band intensity near to 1750 cm^{-1} peak and the presence of broader bands within the range of 2800–4500 cm^{-1}, which were attributed to -OH stretching and to CO and COOH vibrations, respectively.[34] In PLLA degradation process, a band at 1600 cm^{-1} associated with the carboxylate (-COO-) group, formed due to the hydrolytic scission of the ester group, was reported by Larrañaga et al.,[35] however; this band was not observed in our experimental FTIR spectra. Broadening in the hydroxyl (-OH-) peak around 3500 cm^{-1} in Figure 2(B) is evidence of the chemical bonding interaction between the PLA chains and the free Ca^{2+} ions of the Ringer solution which is PLA concentration dependent due to that no broadening is detected in Figure 2(A). However, no evidence of the hydrolysis process in PLA membranes was observed which is associated with the deformation vibration for H–O–H bonds of the physically adsorbed water molecules on PLA fiber localized at 1623 cm^{-1} in the IR spectra, a vibration band that was not detected in any of the spectra.[36]

Scanning electron microscope

Analysis of spun membranes of PLA by SEM revealed that membranes are composed of smooth and uniform fibers with minimal bead formation with random orientation and with diameter size depending in the PLA concentration (7% w/v and 10% w/v, Figure 3). Using image analysis, distributions of fiber diameters were determined before and after *in vitro* degradation test. Fiber diameter demonstrated that the membrane fiber of PLA had an average diameter distribution of approximately 0.558 ± 0.141 μm for 7% w/v and approximately 0.647 ± 0.137 μm for 10% w/v. After *in vitro* degradation, the morphology of the fibers did not exhibit a significant change in terms of fiber diameter in both concentrations of PLA where the average diameter in the bi-distilled water solution were approximately 0.576 ± 0.146 μm for 7% w/v and approximately 0.650 ± 0.148 μm for 10% w/v; while the average diameter in the Ringer solution were approximately 0.633 ± 0.147 μm for 7% w/v and approximately 0.645 ± 0.140 μm for 10% w/v.

Mechanical properties

The mechanical properties of membrane spun from PLA (7% w/v and 10% w/v) are shown in Figure 4. It can be observed that the mechanical properties tested for the PLA 7% w/v scaffold show an elastic modulus of 78.7 ± 6.2 MPa prior to *in vitro* degradation in bi-distilled water,

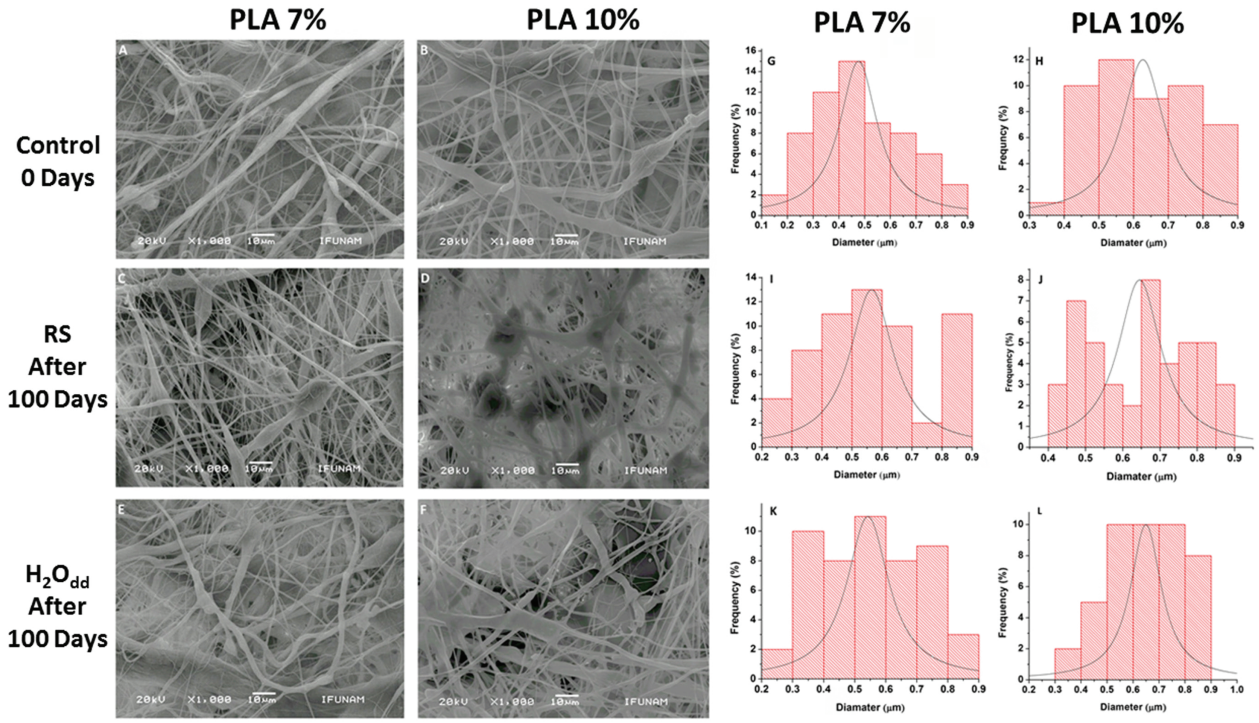

FIGURE 3. SEM images of the fiber morphology and estimation of diameter distribution of fiber size of PLA spun membrane of 7% w/v (A and G) and 10% w/v (B and H) before the *in vitro* degradation test. Images of PLA spun membrane of 7% w/v (C) and 10% w/v (D) of the fiber morphology by SEM and estimation of diameter distribution of fiber size for 7% w/v (I) and 10% w/v (J) after 100 days of *in vitro* degradation in Ringer solution and SEM images of fiber morphology for 7% w/v (E) and 10% w/v (F) and diameter distribution of fiber size for 7% w/v (K) and 10% w/v (L) after 100 days of *in vitro* degradation in bidistilled water.

however, after 100 days of incubation the elastic modulus was of 26.2 ± 8.1 MPa. For PLA 10% w/v the elastic modulus was of 26.2 ± 4.0 MPa prior to *in vitro* degradation in bi-distilled water and after 100 days of incubation, the elastic modulus was of 23.1 ± 1.8 MPa.

On the other hand, for PLA 7% w/v scaffold prior to *in vitro* degradation in Ringer solution, the elastic modulus was of 78.7 ± 6.2 MPa and after 100 days the elastic modulus was of 63.2 ± 6.2 MPa. Likewise, for the PLA 10% w/v scaffold prior to *in vitro* degradation in Ringer solution, the elastic modulus was of 26.2 ± 4.0 MPa and after 100 days of incubation the elastic modulus was of 20.7 ± 4.7 MPa. From the results of the mechanical properties of the PLA spun mat (7% w/v and 10% w/v) it was revealed that the elastic modulus of the membranes drops after incubation when comparing with the spun membranes without any incubation time considered as time zero [Figure 4(A)].

Similar behavior is presented by the resilience of the membranes spun mats before and after 100 days of incubation. The resilience of the membranes spun mats revealed that before *in vitro* degradation in bi-distilled water for the PLA 7% w/v scaffold this was 35.4 ± 5.0 μJ/mm^3 and after 100 days of incubation change its value to 24.8 ± 5.0 μJ/mm^3. For PLA 10% w/v scaffold prior to *in vitro* degradation in bi-distilled water it was 62.3 ± 33.0 μJ/mm^3 and after 100 days of incubation, it was 31.1 ± 5.0 μJ/mm^3.

Moreover, for the PLA 7% w/v scaffold before *in vitro* degradation in Ringer solution, the resilience was 35.4 ± 5.0 μJ/mm^3 and after 100 days of incubation it was 20.7 ± 5.0 μJ/mm^3. For the PLA 10% w/v scaffold before of *in vitro* degradation in Ringer solution the resilience was 62.3 ± 33.0 μJ/mm^3 and after 100 days of incubation it was 20.9 ± 5.0 μJ/mm^3.

The results of resilience of the PLA spun mat (7% w/v and 10% w/v) showed that less energy was needed to achieve maximal elastic deformation after the *in vitro* degradation independently of the concentration of PLA scaffold during the 100 days of incubation in bi-distilled water and Ringer solution [Figure 4(B)].

Biocompatibility

Figure 5 presents the result of the *in vitro* indirect cytotoxic evaluation of hBM-MSC cells after 3, 5, 7, and 9 days of culture. Results demonstrated that the PLA spun membrane scaffolds of 7% w/v and 10% w/v did not release any toxic component that could affect the growth of the cells cultured in comparison with hBM-MSC that were culture with a toxic medium.

Figure 6 showed the cell viability of hBM-MSC cultured onto the surface of the PLA (7% w/v and 10% w/v) fiber spun membranes evaluated by blue formazan accumulation (MTT assay) after 3, 5, 7, and 9 days of culture. Our results demonstrated that cells proliferate in similar levels on PLA 7% w/v and 10% w/v fiber scaffolds during the first period of cell-culture time (3 and 5 days). However, after 7 and 9 days of culture, 10% w/v PLA exhibited better cell

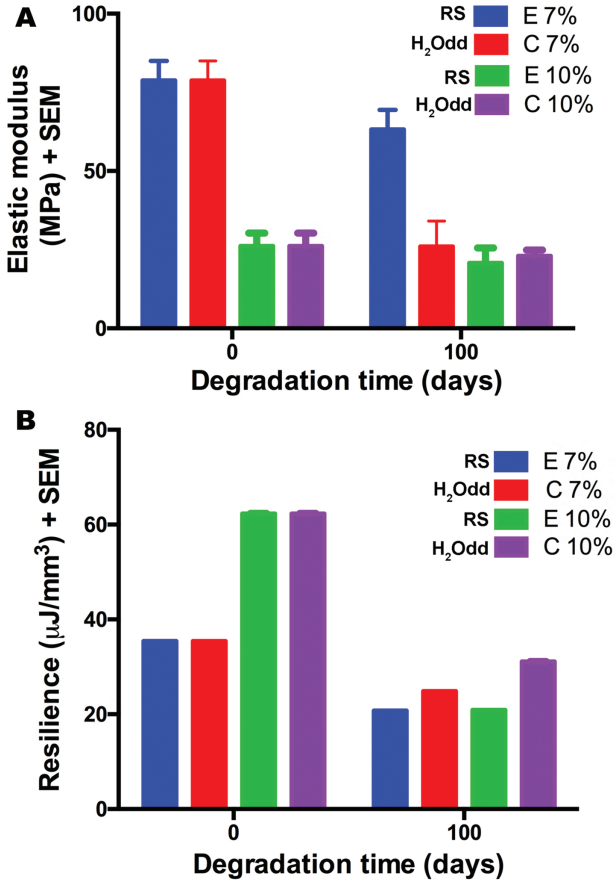

FIGURE 4. Mechanical properties of PLA spun membrane fiber scaffold. (A) Elastic modulus measurement of PLA (7% w/v and 10% w/v) and (B) Resilience behavior of PLA (7% w/v and 10% w/v) before and after 100 days of *in vitro* hydrolytic degradation in bidistilled water and Ringer solution.

proliferation in comparison with the PLA fiber scaffold of 7% w/v with statistical significance at $p < 0.05$. Moreover, the results showed that hBM-MSC cells growing on PLA fiber spun mats during all cell-culture times indicated no presence of cytotoxicity while, contrariwise, these showed a good biocompatibility response to the material.

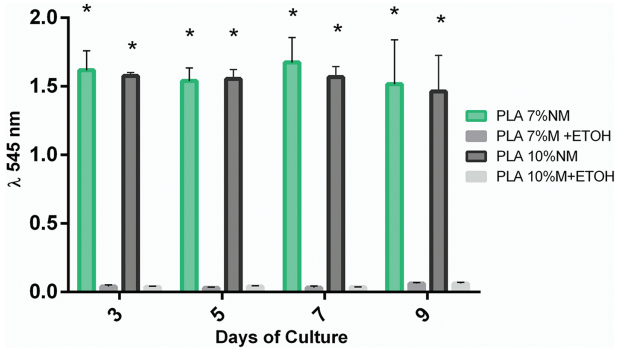

FIGURE 5. Evaluation of the *in vitro* indirect cytotoxicity assay of the eluted solution of PLA spun membrane scaffold (7% w/v and 10% w/v) and medium with 10% of ethanol on hBM-MSC cells.

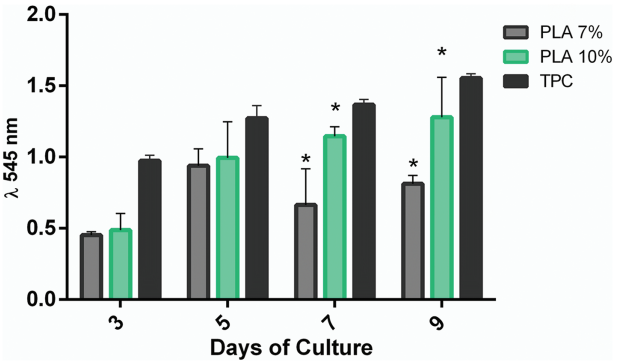

FIGURE 6. Cell viability of hBM-MSC cultured onto 7% w/v and 10% w/v spun membrane fiber scaffold of PLA surface after 9 days of cell culture.

In vivo degradation

Figure 7 presents cross-section photomicrographs of the histological evaluation following subcutaneous implantation of membrane spun mats of PLA (7% w/v and 10% w/v) and the control Gelfoam into the back of adult male Wistar rats at the time points indicated (8–100 days) stained with H&E. From the photomicrographs, the inflammatory infiltrates and the type of tissue surrounding the implanted biomaterials with respect to time could be evaluated. In the first time period (8 days), we could observed in 7% w/v of PLA mild inflammatory infiltrate and dense connective tissue with congestive blood vessels and similar behavior was found on the implanted PLA 10% w/v scaffold; where longitudinal disposition of the collagen fibers was observed. Among these, we observed scarce mononuclear inflammatory infiltrate with vascular congestion in comparison with the control group surrounded by tissue at the same implantation time.

After 20 days of implantation, in the area of 7% w/v PLA membrane scaffold, it was possible to identify a dense and organized collagen fibers with a decrease in the number of blood vessels. For the 10% w/v PLA membrane scaffold it was possible to observe the presence of dense collagen with mononuclear inflammatory infiltrate between the fibers and congestive vessels in the implanted area. Moreover, in the control group (Gelfoam) it was possible to appreciate the presence of a slight inflammatory infiltrate consisting of lymphocytes with the formation of foreign-body giant cells and an irregular collagen deposit with a proliferation of vascular channels.

After 40 days of implantation for the spun membrane of 7% w/v PLA, the sections demonstrated, between the scaffolds a fibrous tissue walls with fiber fragmentation and a few collagen fibers. For the 10% w/v PLA scaffolds in the section, it was observed a dense connective tissue capsules with interstitial edema; while in the intermediate area of the material, there was a deposit of collagen fibers. At the same time, for the control group, a dense connective tissue deposition was observed in the implanted area.

In the cross-section corresponding to 60 days of implantation in the area of the 7% w/v PLA membrane scaffold, we were able to identify a dense connective capsule with

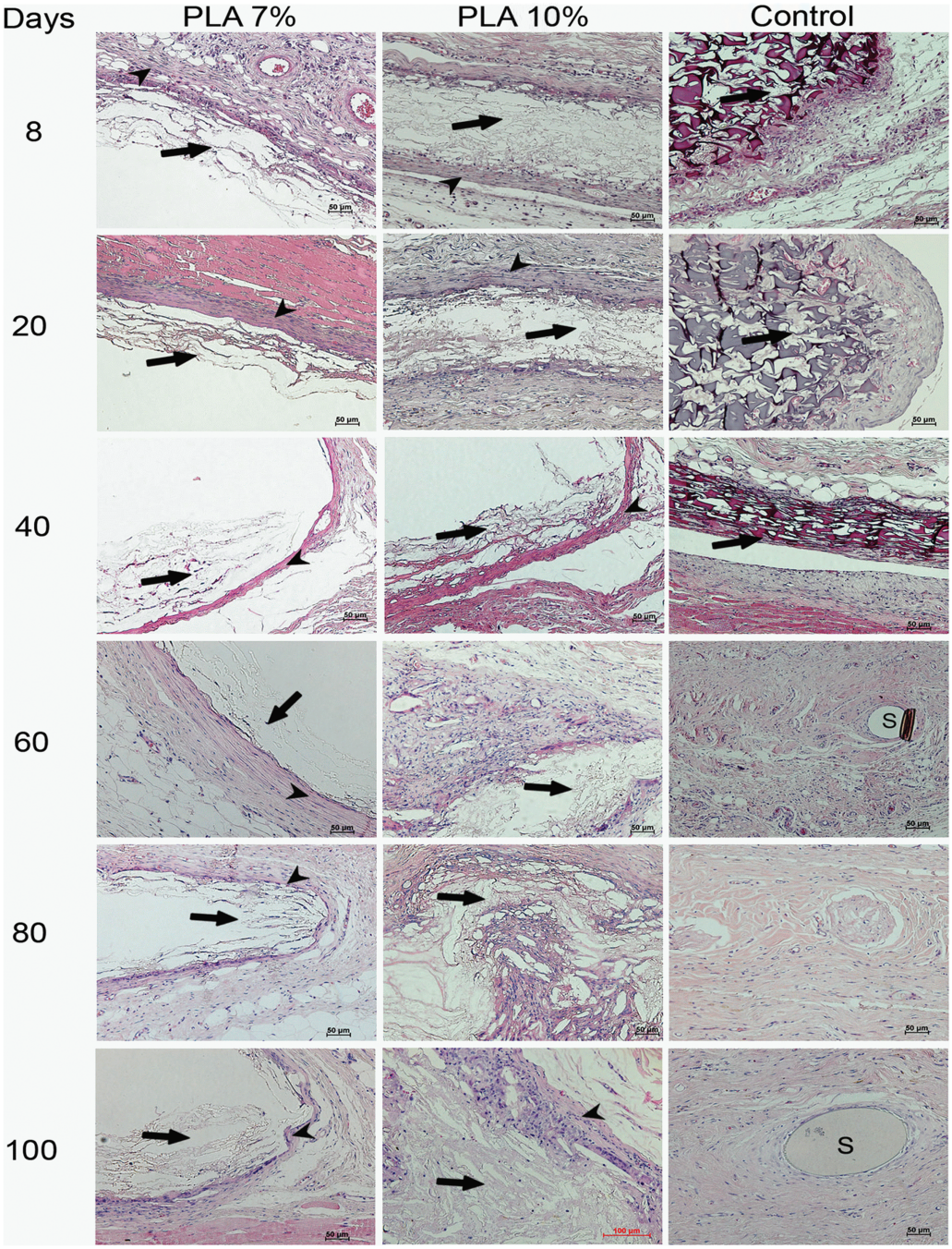

FIGURE 7. Photomicrographs at 20× stained with H&E images of PLA (7% w/v and 10% w/v) and control (Gelfoam) following implantation into the back of adult male Wistar rats at the points indicated (8–100 days) at 20×. The *in vivo* study showed that it is possible to observe the formation of collagen fibers in the space where the material was implanted (arrows). Moreover, from day 20 of *in vivo* implantation is more evidence to observe, surrounding the scaffolds, the formation of dense fibrous connective tissue (arrowheads). Nevertheless, in the photomicrographs corresponding to the spun membrane mats of PLA it is possible to observe the presence of the space of the scaffold in comparison with the Gelfoam and, from day 60 of *in vivo* implantation, only deposits of dense collagen without evidence of the material could be appreciated.

collagen fibers in a horizontal arrangement and, between the materials, we were able to appreciate a small deposit of fibrin. In 10% w/v PLA, an intense inflammatory lymphocytic infiltrate with abundant foreign-body giant cells was identified. Moreover, for the control group, a dense collagen deposit without evidence of Gelfoam or fibrous wall could be appreciated.

At the 80-day time, we observed the presence of a few fibrin bands in the 7% w/v PLA area of implantation and a capsule could be identified in addition to a loose of connective tissue. For the 10% w/v PLA implantation area there was a dense connective tissue deposition of irregular shape and we were able to appreciate irregular collagen fibers between the material with a proliferation of some blood

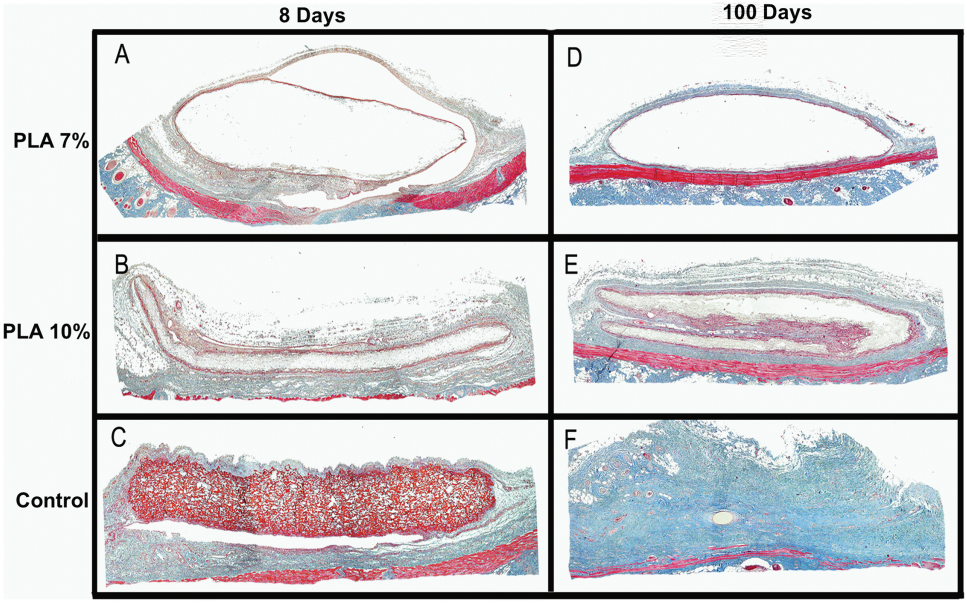

FIGURE 8. Histologic cross-section images of control (Gelfoam) and experimental (PLA 7% w/v and 10% w/v) stained with Masson trichrome at 8 and 100 days after implantation (A). A thin connective tissue wall is observed with light presence of fibrin bands. (B) showed a greater thickening of the capsule with dense connective tissue and on the right side there is a deposit of collagen fibers. It is possible to identify the capsule of dense connective tissue and in the right, there is a presence of the Gelfoam (C). (D) shows the capsule of dense connective tissue. (E) The capsule of dense fibro connective tissue, thickened and irregular and it is observed the presence of deposit of collagen and (F) deposit of mature and dense collagen without evidence of Gelfoam.

vessels without the presence of foreign-body giant cells. In addition, for the control group, there was dense collagen deposition observed in some hyalinized areas.

In the last evaluated period (100 days) in the area of PLA 7% w/v membrane scaffold a dense connective tissue wall with inflammatory lymphocytic infiltrate, a small multinucleated giant cell with a fragmentation of the collagen fibers could be observed in addition to a small fibrin deposit between the material. For the PLA 10% w/v membrane scaffold, we observed a connective tissue wall, while between the material, we could appreciate a dense collagen deposit with proliferations and vascular canals. Finally, for the control (Gelfoam) material, it was possible to identify an area of dense hyalinized collagen with a reduced light of vessels.

Figure 8 depicted the histological sections stained with Masson's trichrome to evaluate tissue deposit surrounding the experimental PLA membrane scaffolds (7% w/v and 10% w/v) and for the control scaffold (Gelfoam) following subcutaneous implantation into the back of adult male Wistar rats at the initial time (8 days) and the final time (100 days). At day 8 a thin, loose connective tissue wall could be observed in the histological samples corresponding to the 7% w/v PLA fiber scaffold. Within the space of the material, we could distinguish a few fibrin bands, and at 100 days of implantation a thickening of the capsule of dense connective tissue was observed in addition to deposition of collagen fibers observed in the material space.

For the histological sections corresponding to the 10% w/v PLA membrane scaffold a capsule of dense connective tissue with abundant deposits of collagen was identified 8 days after implantation. Moreover, after 100 days of implantation of the material, we were able to appreciate irregular collagen depositions with a dense connective tissue.

In the histological sections corresponding to the control (Gelfoam) we could identify, after 8 days of implanted material, fibrous connective tissue and after 100 days of implantation, we were able to identify a dense mature collagen deposit without any evidence of the Gelfoam material because this material had been completely resorbed.

DISCUSSION

Synthesis or fabrication of fiber membrane scaffold in tissue engineering regeneration strategies is attracting more attention for mimicking the ECM. The ECM is often composed of fiber proteins with diameters ranging from tens to hundreds of nanometers. Thus, mimicking the fiber size by artificial matrix has an advantage capable of recapitulating the key features of the ECM that control cell migration, proliferation and differentiation.[37] In view of this, we have been exploring air-jet technology (AJT) as a simple, efficient, and alternative method for the fabrication of nanofiber membrane that can be used as tissue scaffold. This technology has been reported as a one-step low-cost process with high production rate over short time based on the use of pressurized gas, which is dispensed at an extreme speed in order to stretch the polymer solution into thin fibers at the nozzle outlet. At the same instant, the solvent starts to evaporate and continues to do so after the fibers are deposited onto a substrate.[38,39] Our results by SEM characterization demonstrated that we were able to collect and fabricate, by the

AJT, PLA membrane scaffolds with nanometric, random fiber structure, where the concentration of PLA exerts a direct effect on the mean diameter size of the fibers. This nanometric fiber structure could achieve the desirable functionality, mimicking the intricate interaction between cells and their microenvironment with respect to the ECM and our results are in accordance with recent studies using the AJT technology, that report similar fiber diameter structure and validate good biocompatibility properties of these spun mats.[11,16,18] Characterization of chemical and microstructural properties of the synthesized PLA nanofiber scaffolds demonstrated that the membrane presents an amorphous structure that remain amorphous respect to the percent of concentration of the PLA solution. This amorphous phase is in agreement with reports that PLA treated with ethanol afford very broad peak without any sharp crystalline peaks, indicating that the ethanol is not able to induce PLA crystallization.[40] This is important because it has been reported that crystallinity significantly affects the degradability of the polymer *in vivo,* that the degradation time is longer with a high crystallinity phase and that the degree of crystallinity determines the mechanical properties of the polymer.[41,42]

In our study, the evaluation of the mechanical properties before and after *in vitro* degradation test revealed that the elastic modulus was affected. This affection could be a result of the swelling, due to the adsorption of water from the solutions, which causes the widening of the PLA fibers as exhibited in the increase of fiber diameters determined by SEM analysis. Thus, the differences in mechanical properties demonstrated that morphology of fibers membrane scaffold is a determining factor, together with the amorphous structure obtained by the AJT process.

Our analyses showed that PLA scaffolds exhibit amorphous behavior that remains as the PLA concentration increases, which was also shown by Rezabeigi.[43] The elastic deformation of the material increases and the yield stress decreases when the elastic modulus decreases. This combination of elastic properties results in increased scaffold resilience [Figure 4(B)]. This is in accordance with studies reporting that the architecture of the scaffold characterized by its crystallinity, porosity, interconnected pore size, the structural arrangement of molecules forming the fibers, and its morphology, play an important role for ensuring mechanical and degradation stability during the tissue regeneration process.[43,44] This is also supported by study on the effect of crystallinity on the degradation of bioresorbable polyesters reported by Fernández et al.[45] and new polymeric biomaterials for application in the medical field with decreased crystallization capability and enlarged amorphous character of the polymers.[46]

Biocompatibility assessment is a complex procedure that incorporates both *in vitro* and *in vivo* tests directed toward evaluating cytotoxicity, allergic responses, irritation, inflammation, and systemic and chronic toxicity.[47] In our study, the *in vitro* biocompatibility in a static environment to evaluate cytotoxicity probably due to solvent remaining in the structure of the PLA fiber spun mat after being synthesized by AJT that showed that there is no release into the liquid medium after the incubation time (Figure 5). The expected release of the remaining solvent or the expected degradation of the scaffold mainly by ester hydrolysis during the incubation in cell-culture media at 37°C indicated that the PLA membrane scaffold is biocompatible. This asseveration is supported by the viability assay which revealed that hBM-MSC growing on the scaffold indicate a good cellular interaction (Figure 6). Moreover, the viability response of hBM-MSC was influenced by the physical properties of the fibers, such as size-of-scale, geometric architecture, random-fiber orientation and modulation including polymer-concentration changes in the scaffold that directly contributed to the biological-response preferences of the cells on the 10% w/v of PLA scaffold followed by 7% w/v of PLA scaffold after 9 days of culture. Our findings are consistent with those of several studies reporting that physicochemical properties and specific fibrillar microarchitecture; such as that of the ECM microenvironment of biodegradable-polymers scaffolds spun membranes which are desirable for cells, because they could provide mechanical support for cellular interactions that improving the biological responses.[10,48,49]

In the final analysis of *in vivo* studies to investigate the biodegradation properties of PLA spun mat nanofibers (7% w/v and 10% w/v) our results demonstrated only a mild inflammatory tissue reaction after all the time of implantation (100 days) with noticeable differences in terms of degradation between scaffolds. Normally, PLA is subject to biodegradation based on the hydrolytic reaction and its products are considered nontoxic natural metabolites that are eliminated from the body through urine excretion and through the respiratory route. However, it has been reported that, although their degradation products are nontoxic, the latter are acidic in nature, causing a decrease in the local pH, which autocatalytically accelerates the polymer degradation rate and give rise to a more intense inflammatory response.[50] This could be observed in the 10% w/v of PLA nanofiber scaffold which demonstrated more acute inflammatory cell infiltration and the formation of fibrous capsules when increased the implantation time, indicating that nanofiber biodegradation resulted in microenvironmental accumulation of the partial acidic products. However, our study agrees with several reports demonstrating that, after PLA implantation, there is a mild tissue inflammatory response due to degradation of the polymeric phase, considering that this polymer as biocompatible.[51–53] Moreover, several reports indicate that the rate of biodegradability of synthetic polymers that degrade over time depends mainly on the intrinsic properties of the polymer, including chemical structure, the presence of hydrolytically unstable bonds, the crystalline-amorphous ratio, the copolymer ratio level, if applicable, and the initial molecular weight, that it is influenced by physical factors such as the total porosity, pore size distribution, fiber diameter, and chemical factors including the presence of enzymes and the pH at the site of implantation.[24,35,45,46,54,55] This aspect could be important because PLA membrane scaffolds synthesized by AJT were amorphous and the *in vitro* and *in vivo* degradability could

be influenced by the fiber diameter reflected on the mechanical properties indicating changes in the scaffolds properties. However, the scaffolds exhibited dimensional stability during the degradation period time, which is an important prerequisite for materials evaluation for tissue engineering regeneration.[56,57]

CONCLUSION

The production of PLA scaffolds with the AJS technique comprises a good alternative for use in tissue engineering since the results showed that PLA nanofibers, regardless of polymer concentration (7% w/v and 10% w/v) and degradation time (0–100 days) are biocompatible. The *in vivo* studies demonstrated no evidence of toxicity because there is no significant histological response after 100 days. The mechanical evidence indicates that 7% w/v scaffolds are less rigid, therefore, more resistant to stress, thus good candidates for use in hard tissues, in contrast with the 10% w/v scaffolds which could be applied to soft tissues. Finally, 7% w/v and 10% w/v of PLA nanofiber scaffolds fabricated by means of the AJS technique revealed favorable physical and chemical properties for tissue engineering applications. Therefore, the use of these scaffolds requires more studies in order to propose an alternative for research in the biomedical field regarding the development of translational therapies with animals and to evaluate their potential in bone, vascular, or skin tissue regeneration.

ACKNOWLEDGMENTS

Authors want to thank Raul Reyes Ortíz, Adriana Tejeda Cruz, and Omar Novelo from IIM-UNAM for their technical assistance. M.V.G.H. thanks to CONACYT (No. 299078) for his doctoral scholarship during the course of this study as requirement for the degree of Doctor of Science in the Postgraduate in Biological Sciences Program.

REFERENCES

1. Xu W, Shen R, Yan Y, Gao J. Preparation and characterization of electrospun alginate/PLA nanofibers as tissue engineering material by emulsion electrospinning. J Mech Behav Biomed Mater 2017;65:428–438.
2. Tajbakhsh S, Hajiali F. A comprehensive study on the fabrication and properties of biocomposites of poly(lactic acid)/ceramics for bone tissue engineering. Mater Sci Eng C 2017;70:897–912.
3. Fisher MB, Mauck RL. Tissue engineering and regenerative medicine: Recent innovations and the transition to translation. Tissue Eng Part B 2013;19(1):1–13.
4. Kelleher CM, Vacanti JP. Engineering extracellular matrix through nanotechnology. J R Soc Interface 2010;7:S717–S729.
5. Wu K, Zhang X, Yang W, Liu X, Jiao Y, Zhou Ch. Influence of layer-by-layer assembled electrospun poly (l-lactic acid) nanofiber mats on the bioactivity of endothelial cells. Appl Surf Sci 2016; 390:838–846.
6. Rogina A. Electrospinning process: Versatile preparation method for biodegradable and natural polymers and biocomposite systems applied in tissue engineering and drug delivery. Appl Surf Sci 2014;296:221–230.
7. Bhardwa NJ, Kundu SC. Electrospinning: A fascinating fiber fabrication technique. Biotechnol Adv 2010;28:325–347.
8. Hu X, Liu S, Zhou G, Huang Y, Xie Z, Jing X. Electrospinning of polymeric nanofibers for drug delivery applications. J Control Release 2014;185:12–21.
9. Alvarez-Perez MA, Guarino V, Cirillo V, Ambrosio L. Basic protocols to investigate hMSC behavior onto electrospun fibers. Methods Mol Biol 2013;1058:109–117.
10. Guarino V, Cirillo V, Taddei P, Alvarez-Perez MA, Ambrosio L. Tuning size scale and crystallinity of PCL electrospun fibers via solvent permittivity to address hMSC response. Macromol Biosci 2011;11(12):1694–1705.
11. Bienek DR, Hoffman KM, Tutak W. Blow-spun chitosan/PEG/PLGA nanofibers as a novel tissue engineering scaffold with antibacterial properties. J Mater Sci Mater Med 2016;27(9):146.
12. Bonan RF, Bonan PRF, Batista AUD, Sampaio FC, Albuquerque AJR, Moraes MCB, Mattoso LHC, Glenn GM, Medeiros ES, Oliveira JE. In vitro antimicrobial activity of solution blow spun poly(lactic acid)/polyvinylpyrrolidone nanofibers loaded with Copaiba (Copaifera sp.) oil. Mater Sci Eng C 2015;48:372–377.
13. Bilbao-Sainz C, Chiou B-S, Valenzuela-Medina D, Du W-X, Gregorski KS, Williams TG, Wood DF, Glenn GM, Orts WJ. Solution blow spun poly(lactic acid)/hydroxypropyl methylcellulose nanofibers with antimicrobial properties. Eur Polym J 2014;54:1–10.
14. da Costa Farias MR, Rodrigues Menezes R, Oliveira JE, Medeiros ES. Production of submicrometric fibers of mullite by solution blow spinning (SBS). Mater Lett 2015;149:47–49.
15. Sinha-Ray S, Sinha-Ray S, Yarin AL, Pourdeyhimi B. Theoretical and experimental investigation of physical mechanisms responsible for polymer nanofiber formation in solution blowing. Polymer 2015;56:452–462.
16. Oliveira JE, Medeiros ES, Cardozo L, Voll F, Madureira EH, Mattoso LHC, Assis OBG, Odilio Benedito Garrido Assis OD. Development of poly(lactic acid) nanostructured membranes for the controlled delivery of progesterone to livestock animals. Mater Sci Eng C 2013;33:844–849.
17. Zhuang X, Jia K, Cheng B, Guan K, Kang W, Ren Y. Preparation of polyacrylonitrile nanofibers by solution blowing process. J Eng Fibers Fab 2013;8(1):88–93.
18. Tutak W, Sarkar S, Lin-Gibson S, Farooque TM, Jyotsnendu G, Wang D, Kohn J, Bolikal D, Simon CG Jr. The support of bone marrow stromal cell differentiation by airbrushed nanofiber scaffolds. Biomaterials 2013;34(10):2389–2398.
19. Oliveira JE, Moraes EA, Costa RGF, Afonso AS, Mattoso LHC, Orts WJ, Medeiros ES. Nano and submicrometric fibers of Poly(D,L-Lactide) obtained by solution blow spinning: Process and solution variables. J Appl Polym Sci 2011;122:3396–3405.
20. Oliveira JE, Moraes EA, Marconcini JE, Mattoso LHC, Glenn GM, Medeiros ES. Properties of poly(lactic acid) and poly(ethylene oxide) solvent polymer mixtures and nanofibers made by solution blow spinning. J Appl Polym Sci 2013;129:3672–3681.
21. Sinha-Ray S, Zhang Y, Yarin AL, Davis AS, Pourdeyhimi B. Solution blowing of soy protein fibers, Biomacromol 2011;12(6):2357–2363.
22. Saini P, Arora M, Kumar MN. Poly(lactic acid) blends in biomedical applications. Adv Drug Deliv Rev 2016;107:47–59.
23. Murariu M, Dubois P. PLA composites: From production to properties. Adv Drug Deliv Rev 2016;107:17–46.
24. Sabbatier G, Larrañaga A, Guay-Bégin A-A, Fernandez J, Diéval F, Durand B, Sarasua J-R, Laroche G. Design, degradation mechanism and long-term cytotoxicity of poly (L-lactide) and poly (lactide-co-ε-caprolactone) terpolymer film and air-spun nanofiber scaffold. Macromol Biosci 2015;15:1392–1410.
25. Lasprilla AJ, Martinez GA, Lunelli BH, Jardini AL, Filho RM. Polylactic acid synthesis for application in biomedical devices—A review. Biotechnol Adv 2012;30(1):321–328.
26. Montesinos JJ, Flores-Figueroa E, Castillo-Medina S, Flores-Guzmán P, Hernández-Estévez E, Fajardo-Orduña G, Orozco S, Mayani H. Human mesenchymal stromal cells from adult and neonatal sources: Comparative analysis of their morphology, immunophenotype, differentiation patterns and neural protein expression. Cytotherapy 2009;11:163–176.
27. Montesinos JJ, Mora-García M de L, Mayani H, Flores-Figueroa E, García-Rocha R, Fajardo-Orduña GR, Castro-Manrreza ME, Weiss-Steider B, Monroy-García A. In vitro evidence of the presence of mesenchymal stromal cells in cervical cancer and their role in protecting cancer cells from cytotoxic T cell activity. Stem Cells Dev 2013;22:2508–2519.

28. Inai R, Kotaki M and Ramakrishna S. Structure and properties of electrospun PLLA single nanofibers. Nanotechnology 2005;16: 208–213.
29. Gupta KK, Mishra PK, Srivastava P, Gangwar M, Nath G, Maiti P. Hydrothermal in situ preparation of TiO_2 particles onto poly(lactic acid) electrospun nanofibres. Appl Surf Sci 2013;264:375–382.
30. Gartner H, Li Y, Almenar E. Improved wettability and adhesion of polylactic acid/chitosan coating for bio-based multilayer film development. Appl Surf Sci 2015;332:488–493.
31. Krikorian V, Pochan DJ. Crystallization Behavior of poly(l-lactic acid) nanocomposites: Nucleation and growth probed by infrared spectroscopy. Macromolecules 2005;38:6520–6527.
32. Xia X, Liu W, Zhou L, Liu H, He S, Zhu Ch. Study on flax fiber toughened poly (lactic acid) composites. J Appl Polym Sci 2015; 132(18):42573.
33. Wu F, Lan X, Ji D, Liu Z, Yang W, Yang M. Grafting polymerization of polylactic acid on the surface of nano-SiO2 and properties of PLA/PLA-grafted-SiO2 nanocomposites. J Appl Polym Sci 2013; 129(5):3019–3027.
34. Khaliliazar Sh, Akbari S, Kish MH. Modification of poly(l-lactic acid) electrospun fibers and films with poly(propylene imine) dendrimer. Appl Surf Sci 2016;363:593–603.
35. Larrañaga A, Guay-Bégin AA, Chevallier P, Sabbatier G, Fernández J, Laroche G, Sarasua JR Biomatter 2014;4:e27979.
36. Zhang J, Maurer FJH, Yang M. In situ Formation of TiO_2 in electrospun poly(methyl methacrylate) nanohybrids. J. Phys. Chem. C 2011;115(21):10431–10441.
37. Liu W, Thomopoulos S, Xia Y. Electrospun nanofibers for regenerative medicine. Adv Healthce Mater 2012;1:10–25.
38. Abdal-hay A, Sheikh FA, Lim JK. Air jet spinning of hydroxyapatite/poly(lactic acid) hybrid nanocomposite membrane mats for bone tissue engineering. Colloids Surf B Biointerfaces 2013;102: 635–643.
39. Abdal-Hay A, Hamdy AS, Khalil KA, Lim JH. A novel simple one-step air jet spinning approach for deposition of poly(vinyl acetate)/hydroxyapatite composite nanofibers on Ti implants. Mater Sci Eng C Mater Biol Appl 2015;49:681–690.
40. Gao J, Duan L, Yang G, Zhang Q, Yang M, Fu Q. Manipulating poly(lactic acid) surface morphology by solvent-induced crystallization Appl Surf Sci 2012;261:528–535.
41. Tang M, Dong Y, Stevens MM, Williams CK. Tailoringpolylactide degradation: Copolymerization of carbohydrate lactone and S,S-lactide. Macromolecules 2010;43:7556–7564.
42. Kun E, Marossy K. Effect of crystallinity on PLA microbiological behavior. Mater Sci Forum 2013;752:241–247.
43. Rezabeigi E, Wood-Adams PM, Drew RAL. Production of porous polylactic acid monoliths via nonsolvent induced phase separation. Polymer 2014;55:6743–6753.
44. Henriksen SS, Ding M, Vinther Juhl M, Theilgaard N, Overgaard S. Mechanical strength of ceramic scaffold reinforced with biopolymers is comparable to that of human bone. J Mater Sci Mater Med 2011;22:1111–1118.
45. Fernández J, Larrañaga A, Etxeberría A, Sarasua J. R. Effects of chain microstructures and derived crystallization capability on hydrolytic degradation of poly (L-lactide/ε-caprolactone) copolymers. Polym Degrad Stab 2013;98:481–489.
46. Fernández J, Larrañaga A, Etxeberría A, Wang W, Sarasua JR. A new generation of poly (lactide/ε-caprolactone) polymeric biomaterials for application in medical field. J Biomed Mater Res Part A 2014;102A:3573–3584.
47. Katti DS, Lakshmi S, Langer R, Laurencin CT, Toxicity, biodegradation and elimination of polyanhydrides. Adv Drug Deliv Rev 2002;54:933–961.
48. Kai D, Liow SS, Loh XJ. Biodegradable polymers for electrospinning: Towards biomedical applications. Mater Sci Eng C Mater Biol Appl 2014;45:659–670.
49. Chen W, Ma J, Zhu L, Morsi Y, El-Hamshary H, Al-Deyab SS, Mo X. Superelastic, superabsorbent and 3D nanofiber-assembled scaffold for tissue engineering. Colloids Surf B Biointerfaces 2016; 142:165–172.
50. Gomes ME, Reis RL. Biodegradable polymers and composites in biomedical applications: From catgut to tissue engineering. Part 1 Available systems and their properties. Int Mater Rev 2004;49(5), 261–273.
51. Danoux ChB, Barbieri D, Yuan H, de Bruijn JD, van Blitterswijk CA, Habibovic P. In vitro and in vivo bioactivity assessment of a polylactic acid/hydroxyapatite composite for bone regeneration. Biomatter 2014;4, e27664.
52. Shalumon KT, Chennazhi KP, Tamura H, Kawahara K, Nair SV, Jayakumar R. Fabrication of three-dimensional nano, micro and micro/nano scaffolds of porous poly(lactic acid) by electrospinning and comparison of cell infiltration by Z-stacking/three-dimensional projection technique. IET Nanobiotechnol 2012;6(1): 16–25.
53. Athanasiou KA, Niederauer GG, Agrawal CM. Sterilization, toxicity, biocompatibility and clinical applications of polylactic acid/polyglycolic acid copolymers. Biomaterials 1996;17:93–102.
54. Ye WP, Du FS, Jin WH, Yang JY, Xu Y. In vitro degradation of poly(caprolactone), poly(lactide) and their block copolymers: Influence of composition, temperature and morphology. React Funct Polym 1997;32(2):161–168.
55. Chung S, King MW. Design concepts and strategies for tissue engineering scaffolds. Biotech Appl Biochem 2011;58(6):423–438.
56. Muerza-Cascante ML, Haylock D, Hutmacher DW, Dalton PD. Melt Electrospinning and its technologization in tissue engineering. Tissue Eng Part B 2015;21(2):187–202.
57. Narayanan G, Vernekar VN, Kuyinu EL, Laurencin CT. Poly (lactic acid)-based biomaterials for orthopaedic regenerative engineering. Adv Drug Deliv Rev 2016;107:247–276.